Conformational and Orientational Guidance of the Analgesic Dipeptide Kyotorphin Induced by Lipidic Membranes: Putative Correlation toward Receptor Docking

Sílvia C. D. N. Lopes,[†] Cláudio M. Soares,[‡] António M. Baptista,[‡] Erik Goormaghtigh,[§] Benedito J. Costa Cabral,[||,⊥] and Miguel A. R. B. Castanho*,[||]

Centro de Química-Física Molecular, Instituto Superior Técnico, Av. Rovisco Pais, 1049-001 Lisboa, Portugal, Instituto de Tecnologia Química e Biológica, Universidade Nova de Lisboa, Av. da República, EAN, Apartado 127, 2781-901 Oeiras, Portugal, Structural Biology and Bioinformatics Center, Structure and Function of Biological Membranes Laboratory, CP206/2, Free University of Brussels, Bld du Triomphe, B-1050 Brussels, Belgium, Departamento de Química e Bioquímica da Faculdade de Ciências da Universidade de Lisboa, Campo Grande, Ed. C8, 1749-016 Lisboa, Portugal, and Grupo de Física Matemática da Universidade de Lisboa, Av. Prof. Gama Pinto 2, 1649-003 Lisboa, Portugal

Received: July 4, 2005; In Final Form: November 29, 2005

The analgesic dipeptide kyotorphin (L-Tyr-L-Arg) and an acylated kyotorphin derivative were studied by a combination of theoretical (molecular dynamics simulation and quantum mechanics methods) and experimental (fluorescence and infrared spectroscopies) approaches both in solution and in model systems of membranes. At biological pH the peptides have a neutral net charge. Nevertheless, their phenolic rings interact with phospholipid molecules (partition coefficient varies from 6×10^2 to 2×10^4, depending on the lipid and pH used) despite being exposed to the aqueous bulk medium. The lowest energy transition dipole moment is displaced from the normal to the lipid bilayer by 20° on average. The observed extensive interaction, pK_a, precise location, and well-defined orientation in membranes combined with the ability to discriminate rigid raftlike membrane domains suggest that kyotorphin meets the structural constraints needed for receptor−ligand interaction. The acylated kyotorphin derivative mimics kyotorphin properties and represents a promising way for entrapment in a drug carrier and transport across the blood−brain barrier.

Introduction

Kyotorphin (KTP) is an analgesic dipeptide (L-Tyr-L-Arg; Figure 1) that was first isolated from bovine brain.[1] This dipeptide was subsequently found in the brains of mice, guinea pigs, rabbits, rats, ground squirrels, and humans.[2,3] It acts as a neurotransmitter/neuromodulator in nociceptive responses in the central nervous system,[4] having an approximately 4.2 times higher analgesic effect than endogenous opioid peptides such as Met-enkephalines.[5,6] Despite its opioid activity, several works point out the possibility of an indirect action of KTP, which would not bind to δ, μ, or κ opioid receptors[7] but rather to specific KTP receptors.[8,9] Two mechanisms have been proposed for such a potent analgesic activity in the brain: (1) the activation of KTP receptors induces release of Met-enkephalin and activates a δ-opioid receptor;[8,9] (2) KTP is degraded quickly by KTPases into L-arginine, which is a potent substrate for nitric oxide synthase, then NO is formed and induces the release of Met-enkephalin.[10,11] However, in the pheripheral nervous system, KTP has a nonopioid analgesic effect,[12] which makes it quite appealing for chronic pain treatment, and moreover it inhibits cell proliferation, indicating that peripherical tissue cells also contain KTP receptors.[13] Nevertheless, its pharmacological potential is rather limited. In fact, when KTP is introduced systematically it shows only brief activity and at a high dose of 200 mg/kg.[14] The main problem is the blood−brain barrier (BBB), which only allows compounds with sufficient lipophilicity to cross and also the susceptibility of KTP to various lytic enzymes. Nevertheless, despite the *in vivo* functional studies, structural information about this intriguing dipeptide's mode of action at the molecular level is missing. KTP is a promising molecule for effective therapeutic approaches, but this lack of information hinders pharmacological applications. A logical strategy to target KTP to the brain is the chemical modification of KTP into analogues that are able to maintain analgesic properties and are able to cross the BBB, namely, through association with a drug carrier system.[15] However these analogues must not perturb the "natural" approach to the receptor with favorable orientation and correct exposure. Direct interaction of ligands with the lipidic matrix of membranes plays an important role for this purpose.[16] In the "membrane catalysis" model, Sargent and Schwyzer proposed that peptides would interact with membrane lipids to adopt the necessary conformation for docking cell receptors.[16] In this way the molecular mechanism of receptor-mediated processes is based both on receptor and on membrane requirements. Moreover the interaction of a drug candidate with biological membranes is an important aspect of preclinical drug discovery, because the bioavailability of drugs depends largely on their solubility in cell membranes[17] and the ability to quantify this property facilitates drug design and screening methods. We have chosen to perform the hydrophobization of KTP with a fatty acid residue (palmitoyl) derivatization since this strategy has been proved useful to enhance both the binding and the uptake of proteins

* Author to whom correspondence should be addressed. E-mail: castanho@fc.ul.pt.
[†] Instituto Superior Técnico.
[‡] Universidade Nova de Lisboa.
[§] Free University of Brussels.
[||] Departamento de Química e Bioquímica, Universidade de Lisboa.
[⊥] Grupo de Física Matemática, Universidade de Lisboa.

10.1021/jp053651w CCC: $33.50
Published on Web 02/01/2006

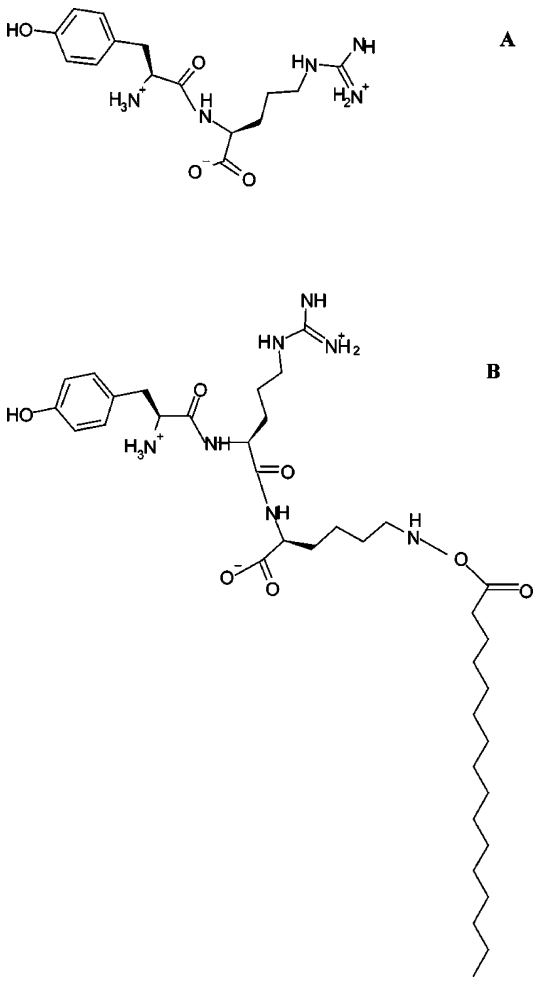

Figure 1. KTP structure at pH < pK_a (A) and of KTP-K-palmitoyl (B).

in cells and is a promising approach for the brain delivery of peptides with a reduced immunogenicity and decreased risk of complications in therapy.[18]

In this work our goals were: (1) to report structural information on the KTP tyrosine moiety both in aqueous solution and in interaction with a model system of biological membranes because tyrosine moieties are crucial factors both for the interaction with cell receptors and for biological activity, as observed for enkephalin peptides;[19] (2) to compare such information to that obtained for a hydrophobic KTP derivative (L-Tyr-L-Arg-L-Lys-ϵ-NH_2-palmitoyl; KTP-K-palmitoyl; Figure 1), which is promising for entrapment in a drug carrier and crossing of the BBB. Moreover this information may be useful to design transporters/receptor-targeted drug delivery systems in an efficient way.

2. Materials and Methods

Kyotorphin (KTP) (Bachem, Switzerland), L-tyrosine (L-Tyr), cholesterol, cholesterol bromide, and 5-methoxy-indole (Sigma, St. Louis, MO) were 99% pure. KTP-K-palmitoyl (Alta Bioscience, England) was 97% pure.

Q-Sepharose and SP-Sepharose resins used for the determination of pK_a were from Amersham Biosciences (Germany) with 3−11 and 4−13 operational pH ranges, respectively. Acetate (20 mM) and Bis−Tris propane buffers (both 20 mM) were used in the pH ranges 4−6 and 6−9.5, respectively, in batch titration studies. HEPES (20 mM) buffer and Bis−Tris propane (20 mM) buffer were used in all other studies, at pH 4.94 and pH 7.4, respectively. All lipids were from Avanti Polar Lipids (Alabaster, AL), and the solvents were spectroscopic grade from Merck (Darmstadt, Germany).

UV−vis absorption measurements were carried out in a Shimadzu spectrophotometer (model UV-3101 PC). A spectrofluorimeter (SLM-Aminco 8100) was also used equipped with a 450 W Xe Lamp and double monochromators in both excitation and emission as well as a quantum counter. Kyotorphin excitation and emission wavelengths were, respectively, 277 and 303 nm.

2.1. Quantum Yield. The relative quantum yield of KTP was determined using 5-methoxy-indole (5-MeOI) in aqueous solution as a reference ($\Phi_F = 0.28 \pm 0.01$).[20] Polarizers, at the "magic angle" orientation, were used with a lipidic (vesicles) suspension to avoid anisotropic effects. All measurements were carried out at room temperature.

2.2. Ionization State of KTP: pK_a Determination. Typical acid−base titration techniques revealed not to be sensitive enough for pK_a determination of KTP. Instead we used a batch technique making use of SP-Sepharose Fast Flow and Q-Sepharose Fast Flow, which are cationic and anionic exchange resins, with sulfopropyl ($-CH_2CH_2CH_2SO_3^-$) and a quaternary ammonium ($-CH_2N^+(CH_3)_3$) as the functional groups, respectively. The rationale of the technique is that if KTP is positively (or negatively) charged at a given pH (which has to be in the operational pH of the resins), then it will bind to cationic (or anionic) exchange resin. However, if KTP is neutral, then it will not bind to any resin. The resins were left to equilibrate overnight at each of the selected pH values. KTP addition was carried out afterward to a final concentration of 4×10^{-4} M. After incubation for 60 min, the samples having different concentrations of the resins were centrifuged for 5 min at 2000*g*. The supernatant was separated for electronic absorption measurements.

The binding of a tyrosine moiety to a resin and its protonation/deprotonation are depicted in Scheme 1

SCHEME 1: Multiequilibrium of Tyrosine Ions

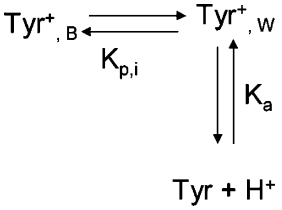

where subscript B refers to resin-bound solute and W to unbound solute. The partition coefficients involved in these multiequilibria are

$$K_{p,i} = \frac{X_{Tyr^+,B}}{X_{Tyr^+,W}} \quad (1)$$

$$K_a = \frac{X_{Tyr}}{X_{Tyr^+,W}} \times 10^{-pH} \quad (2)$$

where X_i are the molar fractions of species *i*.

Resins are usually characterized by a certain capacity,[21] K' (eq 3), which is related to an apparent global equilibrium constant, $K_{p,app}$, accounting for the fraction bound solute per unit mass of the resin (eq 4)

$$K' = \frac{X_{Tyr^+,B}}{X_{Tyr^+,W} + X_{Tyr}} \quad (3)$$

$$K_{p,app} = \frac{K'}{C_r} \quad (4)$$

where C_r is the mass concentration of the resin.

An equivalent but more practical formulation of $K_{p,app}$ is

$$K_{p,app} = \frac{C_{Tyr^+,r}}{[Tyr^+]_W + [Tyr]} \quad (5)$$

where $C_{Tyr^+,r}$ is the concentration of bound solute in moles per resin mass and $[Tyr^+]_W$ and [Tyr] are the molar concentrations of ionized tyrosine in water and neutral tyrosine, respectively. $K_{p,app}$ was experimentally calculated for each of the resins used in this work. $K_{p,app} \cong 0.02$ dm^3/g, which is comparable to other values available in the literature.[21]

Combining eqs 3, 4, and 6 (below), eq 7 is derived

$$X_{Tyr} + X_{Tyr^+,W} + X_{Tyr^+,B} = 1 \quad (6)$$

$$X_{Tyr} + X_{Tyr^+,W} = \frac{1}{K_{p,app} \times C_r + 1} \quad (7)$$

where the left term is the experimentally accessible (UV−vis absorption at $\lambda = 277$ nm) fraction of unbound tyrosine species. $K_{p,app}$ is constant for any given pH value, so eq 6 can be used to describe the dependence of the measurable quantity $X_{Tyr} + X_{Tyr^+,W}$ on C_r. When one seeks the dependence on pH, the relationship between $K_{p,app}$ and pH has to be accounted for. Combining eqs 1−4 leads to

$$X_{Tyr} + X_{Tyr^+,W} = \frac{1}{\frac{K_{p,i}}{1 + K_a \times 10^{pH}} + 1} \quad (8)$$

Because $K_{p,i}$ is constant for any given C_r, this equation can be used to describe the dependence of the measurable quantity $X_{Tyr} + X_{Tyr^+,W}$ on pH. Therefore pK_a can be calculated from the nonlinear regression fitting of $X_{Tyr} + X_{Tyr^+,W}$ versus pH at constant C_r.

The cationic and anionic exchange resin parameters were tested for fluorescein partition. Fluorescein has an associated phenolic ring in its structure and has a high quantum yield. There was a high extent of fluorescein partition to both resins, and with a concentration of 43 g/dm^3 of resin only 15% of fluorescein was unbound.

2.3. Fluorescence Decays. Fluorescence decay measurements were carried out with a time-correlated single-photon counting system. For excitation of the systems with KTP (or KTP-K-palmitoyl) at 285 nm, a frequency-doubled, cavity-pumped dye laser of Rhodamine (Rho), synchronously pumped by a mode-locked Ar^+ laser (514.5 nm, Coherent Innova 400-10) was used. The emission wavelength was 308 nm, and a Hamamatsu R-2809 MCP photomultplier was used for the detection. A Corion W-305-S filter was used to avoid excitation light scattering interference with the measurements.

Large unilamellar vesicles (LUV) (5 mM) were obtained by the extrusion method.[22] KTP (or KTP-K-palmitoyl) solution was added to obtain a final concentration of 70 μM. Fluorescence decays were complex and described by a sum of three exponentials. The mean lifetime, $\bar{\tau}$, was obtained from eq 9.[23]

$$\bar{\tau} = \frac{\sum a_i \tau_i^2}{\sum a_i \tau_i} \quad (9)$$

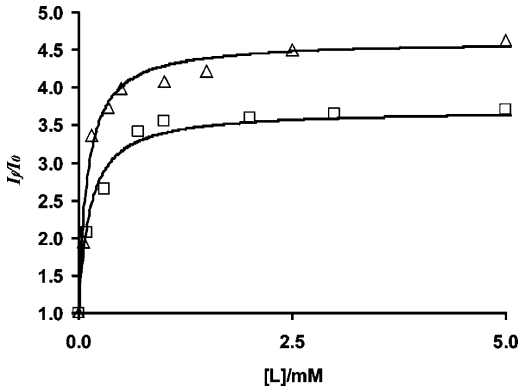

Figure 2. Partition curve of KTP (□) and KTP-K-palmitoyl (△) in POPC LUVs at pH 4.94. Solid lines represent fitting of eq 10 to the data.

2.4. Extent of Incorporation in Lipidic Membranes: Partition Studies. Partition studies were carried out in LUVs, prepared as described before, using different lipid (or lipid + cholesterol) concentrations up to a final concentration of 10 mM. The dipeptide concentration was kept constant (70 μM). The fluorescence intensity was measured with $\lambda_{exc} = 277$ nm and $\lambda_{em} = 303$ nm. The measured fluorescence intensity, I_f, is a balance between the fluorescence intensities of the peptide in the bulk aqueous phase (I_W) and inserted in the lipidic matrix (I_L) (eq 10).[24] The weight factors in this balance depend on the partition coefficient, K_p, which was calculated as a fit parameter in a nonlinear regression methodology (Figure 2). γ_L denotes the molar volume of the lipid used.

$$\frac{I_f}{I_W} = \frac{1 + K_p \gamma_L [L](I_L/I_W)}{1 + K_p \gamma_L [L]} \quad K_p = \frac{[KTP]_L}{[KTP]_W} \quad (10)$$

[L] is the lipid concentration, and subscripts L and W refer to the lipidic and bulk aqueous media, respectively.

The fraction of the fluorescence intensity emitted by the peptide incorporated in the membrane (f_L) can be calculated by

$$f_L = \frac{(I_L/I_W) K_p \gamma_L [L]}{1 + (I_L/I_W) K_p \gamma_L [L]} \quad (11)$$

Details regarding this methodology can be found elsewhere.[24]

2.5. Exposure of the Tyrosine Residue: Fluorescence Quenching Studies. Differential quenching studies were performed to study the in-depth location of KTP in LUVs (prepared as in ref 22) of lipid with or without cholesterol. Namely, KTP fluorescence (dipeptide final concentration 70 μM) was quenched by cholesterol bromide in LUVs of lipid + cholesterol with increasing concentrations of cholesterol bromide. Bromide quencher is replacing the −OH group in cholesterol and is putatively located at the same depth in the lipidic bilayer interface. Quenching studies were performed in systems without cholesterol by adding small aliquots of KI (0.1 M) to the suspension of LUVs with previously added KTP. Briefly, the methodology to ascertain the location of the phenolic ring is based on the dependence of quenching extent on the local concentration of the quencher in the vicinity of the fluorophore. I^- is able to quench fluorophores exposed to the bulk phase, and cholesteryl bromide is a quencher of fluorophores more deeply inserted in the interface. The data treatment was performed as described in ref 25. Fluorescence intensity was measured with excitation and emission wavelengths of 277 and 303 nm, respectively.

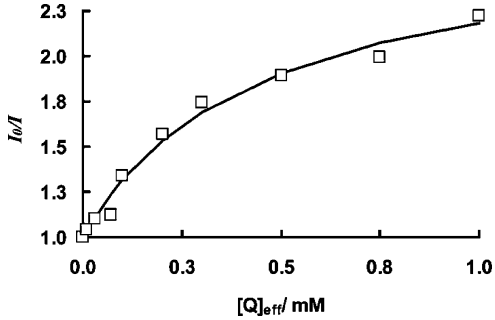

Figure 3. Stern−Volmer plot for the fluorescence quenching of KTP by cholesteryl bromide in the presence of vesicles of POPG + cholesterol (□) (33 mol % of sterol (cholesterol + cholesteryl bromide)) LUVs. Values of the quencher concentration refer to its effective concentration in the lipidic volume. Solid line represents fitting of eq 13 to the data.

The simplest model that describes dynamic or static fluorescence quenching leads to linear Stern−Volmer plots

$$\frac{I_0}{I} = 1 + K_{SV}[Q] \tag{12}$$

where I_0 and I denote the fluorescence intensities in the absence and in the presence of quencher, respectively, K_{SV} is the Stern−Volmer constant, and [Q] is the quencher concentration. However nonlinear Stern−Volmer plots are observed when there are multiple classes of fluorophores in the work by Castanho and Prieto[26] (Figure 3). Considering that there is a fluorophore population protected from the contact of the quencher (A) and a population that is accessible to it (B), the Lehrer equation can be used to fit quenching data[27]

$$\frac{I_0}{I} = \frac{1 + K_{SV}[Q]}{(1 + K_{SV}[Q]) \times (1 - f_B) + f_B} \tag{13}$$

where f_B is the fraction of total emitted light due to subpopulation B

$$f_B = \frac{I_0^B}{I_0} \tag{14}$$

A more detailed description for the interpretation of quenching results can be found in ref 25.

2.6. Orientation of Tyrosine Residues Relative to the Membrane: UV−Vis Linear Dichroism Studies. Samples of aligned lipid multilayers (with or without cholesterol) were obtained by slow evaporation of the solvent as described in ref 28. The final molar ratios of lipid to KTP (or KTP-K-palmitoyl) and lipid to cholesterol to KTP (or KTP-K-palmitoyl) were 2.5:1 and 1.5:1:1, respectively.

The probability density functions, $f(\psi) \sin \psi$, were calculated by means of eq 15

$$f(\psi) \sin \psi = \frac{\exp[\lambda_2 P_2(\cos \psi) + \lambda_4 P_4(\cos \psi)]}{\int_0^\pi \sin \psi \exp(\lambda_2 P_2(\cos \psi) + \lambda_4 P_4(\cos \psi))\, d\psi} \sin \psi \tag{15}$$

A full description is available in the Supporting Information.

2.7. Molecular Dynamics Simulations: Conformers and Ionization State. From both experimental and computational studies, it has been known for quite some time that short peptides do not usually display a unique conformation in aqueous solution but rather an ensemble of interconverting conformations.[29] Thus, the structural characterization of a short peptide involves determining its conformer populations rather than finding an overwhelmingly predominant structure (as done with larger molecules such as proteins). This structural characterization is further complicated by pH effects when titrating groups are present, a problem very clearly illustrated by enkephalin peptides (e.g., see the work by Aburi and Smith[30] and references therein). A similar situation may arise with KTP (see below), and therefore the study of its conformational preferences should consider the presence of different ionization states.

In KTP, the protonation state at physiological pH of the four protonatable groups is obvious, except for the case of the N-terminus. The C-terminus is rather exposed, so it should be deprotonated, bearing a negative charge. The same happens to the side chain of arginine, which given its high pK_a in solution should be protonated, bearing a positive charge. The side chain of tyrosine, for the same reasons, should be protonated and neutral. However, the usual pK_a of an N-terminus is 7.5, so given possible complex influences between groups its protonated state is difficult to predict without further analysis. This is a matter of considerable importance, given that a positively charged N-terminus renders KTP positively charged, while a neutral N-terminus renders it neutral, thus interfering with membrane interaction.

The estimation of protonated states of ionizable groups in solution in proteins and peptides is usually done with a combination of continuum electrostatic and Monte Carlo methods (see ref 31 for a recent review). These methods require a certain number of approximations but are considerably fast and sufficiently reliable if properly used. One of these approximations is to consider the molecules rigid; the only difference between different protonated states is then the existence of the proton itself. While this may be a good approximation for large molecules with low conformational reorganization, it can be problematic for peptides, given their large mobility. With our studies on KTP we have found that this is indeed a problem, given that the N-terminus protonated and deprotonated conformational states of KTP can be considerably different (see below). A possible approach to handle this problem is the linear response approximation (LRA),[32] where conformational ensembles for both states (in this case the protonated and deprotonated states of the N-terminus) are used to estimate the titration behavior of the real titrating species in solution that has an equilibrium of protonatable and conformational states. The theory used in this work is rather similar to the one used by Warshel et al.,[33,34,35] being clearly explained in a recent paper by Eberini et al.[36] Furthermore, instead of the microscopic or semi-microscopic electrostatic methods used by Warshel et al., we here use a continuum electrostatic model (as in the work by Eberini et al.).

The *effective* pK_a of a given protonatable group can be calculated for each peptide conformation obtained in the two simulations using the different protonated states of the N-terminus

$$pK_a = \mathrm{pH} + \log\left(\frac{f}{1 - f}\right) \tag{16}$$

where f is the protonation fraction of a given site at each considered pH.

According to the theory used here the effective pK_a of the N-terminus, at a given value of pH, can be calculated using

$$pK_a = \frac{1}{2}[\langle \mathrm{p}K_a(c)\rangle_P + \langle pK_a(c)\rangle_D] \tag{17}$$

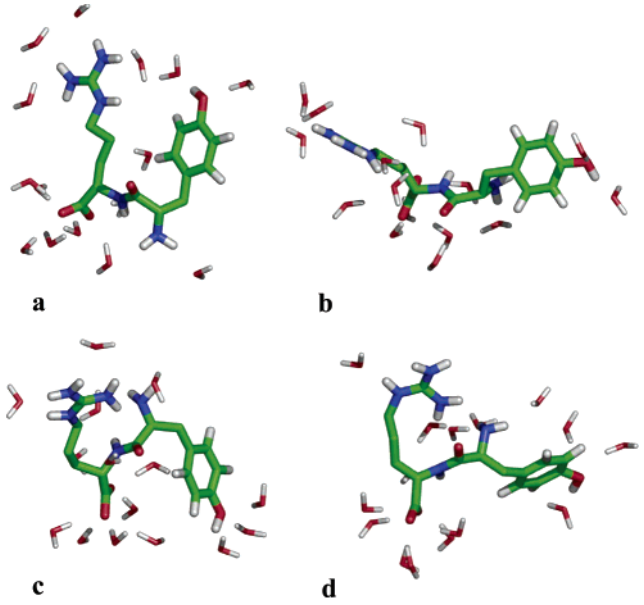

Figure 4. Representative KTP conformations from clusters obtained from the simulation with the neutral N-terminus, having occurrence frequencies of (a) 33.6%, (b) 8.6%, (c) 5.2%, and (d) 8.9%. Water molecules at hydrogen bonding distance were included in the figures as well, since they were used in the infrared spectra calculations.

where c denotes a given conformation of the peptide and P and D denote the protonated and deprotonated ensembles. In this case, ensemble averages of the effective pK_a are calculated for both populations, and the final effective pK_a is calculated using these ensemble averages. Using these values of effective pK_a calculated at different values of pH one can calculate the pK_{half}, i.e., the pH corresponding to half-titration, which is the value that we are looking for to compare with experimental data.

2.8. Quantum Mechanics Simulations: Theoretical Vibrational Studies. The vibrational spectrum of KTP interacting with water was investigated by density functional theory (DFT).[37] Initially, we have selected some structures corresponding to different conformations of KTP in water (Figure 4), which were extracted from the molecular dynamics simulations. The optimization of the structures was then carried out by considering a few (3 or 4) water molecules in close interaction with KTP. By adoption of this "microsolvation" approach, it is expected that the main effect of the water molecules on the vibrational spectrum of KTP is adequately taken into account. Three structures related to the optimized conformers of Figure 4 were considered. The first two structures are similar to conformer 4a, which according to molecular dynamics simulations occurs with a larger frequency (33.6%). In the first one, two water molecules are in close interaction with the carbonyl groups, and two others are close to the phenol O−H group. In the second optimized structure (also similar to conformer 4a), three hydrogen-bonded molecules interact with the KTP molecule, forming one O···H hydrogen bond of 1.92 Å involving the phenol O−H group and one water molecule. This conformer is also stabilized by the interaction of a water molecule with a terminal NH_2 group, leading to a N−H···OH_2 hydrogen bond of 2.10 Å. The third optimized structure is similar to conformer 4b. It is stabilized by the interaction of the phenol O−H group with three water molecules, which contribute, essentially, to modify the vibrational modes related to the phenol ring.

The theoretical calculations were carried out with the hybrid B3LYP functional, which is a combination of the Becke's three-parameter exchange functional (B3)[38] with the Lee, Yang, and Parr (LYP)[39] correlation functional. The 6-31G(d,p)[40] basis set was used in all of the calculations. Geometries were fully optimized. Subsequent frequency calculations characterized the structures as local minima on the potential energy surface; i.e., all frequencies are real. B3LYP/6-31G harmonic frequencies were scaled by 0.9806,[41] an empirical factor proposed to take into account deviations from harmonicity.

The vibrational spectrum of KTP in interaction with water seems to be very dependent on the conformations. The first structure, similar to conformer 4a, is characterized by an intense ν_{O-H} vibrational frequency of 3132 cm^{-1} related to the phenol O−H vibration. This mode involves the coupling with one water molecule in close interaction with KTP. The second most intense vibrational mode corresponds to a ν_{N-H} vibrational frequency of 2793 cm^{-1}, which is possibly related to intramolecular proton transfer between carbonyl and NH groups. As should be expected, the vibrational spectrum of the second optimized structure is not very different from that of the first one. The most intense vibrational mode for the second conformer similar to 4a is again associated with intramolecular proton transfer involving close carbonyl and N−H groups, which leads, in this case, to a ν_{N-H} frequency of 2704 cm^{-1}. This structure is also characterized by a ν_{O-H} frequency of 3254 cm^{-1}, which corresponds to typical O−H bond stretching vibrations of interacting water molecules.

The vibrational spectrum of the third optimized structure exhibits a strong ν_{O-H} frequency of 3061 cm^{-1} related to the interaction of the phenol O−H group with water. This value is quite similar to that observed for the water tetramer and reflects the well-known feature that the phenol O−H group plays a role quite similar to that of one water molecule.

2.9. Attenuated Total Reflection Fourier Transform Infrared Studies. Attenuated total reflection Fourier transform infrared (ATR-FTIR) spectra were obtained on a Bruker IFS55 FTIR spectrophotometer (Ettlingen, Germany) equipped with a mercury−cadmium−telluride (MCT) detector (broad band 12 000−420 cm^{-1}, liquid N_2 cooled, 24 h hold time) at a resolution of 2 cm^{-1} with an aperture of 3.5 mm and acquired in the double-sided, forward−backward mode. The spectrometer was placed on vibration-absorbing sorbothane mounts (Edmund Industrial Optics, Barrington, NJ). Two levels of zero filling of the interferogram prior to Fourier transform allowed encoding the data every 1 cm^{-1}. The spectrometer was continuously purged with dry air (Whatman 75-62, Haverhill, MA). For better stability, the purging of the spectrometer optic compartment (5 L/min) and of the sample compartment (10−20 L/min) were dissociated and controlled independently by flowmeters (Fisher Bioblock Scientific, Illkirch, France). The internal reflection element was a 52 × 20 × 2 mm^3 trapezoidal germanium ATR plate (ACM, Villiers St Frédéric, France) with an aperture angle of 45°, yielding 25 internal reflections. The germanium crystals were washed in Superdecontamine (Intersciences, AS, Brussels, Belgium), a lab detergent solution at pH 13, rinsed with distilled water, washed with methanol, and then with chloroform and finally placed for 2 min in a plasma cleaner PDC23G (Harrick, Ossining, NY) working under reduced air pressure. The germanium crystal was then placed in an ATR holder for a liquid sample with an inlet and outlet (Specac, Orpington, U. K.). The liquid cell was placed at a 45° incidence on a Specac vertical ATR setup. A KRS-5 polarizer was mounted on an automatic rotational changer. Backgrounds of the internal reflection element were collected for each polarization and subtracted from the sample spectra afterward. A total of 256 scans were averaged for each spectrum to improve the signal-to-noise ratio. The final molar ratios of lipid to KTP (or KTP-K-palmitoyl) and lipid to

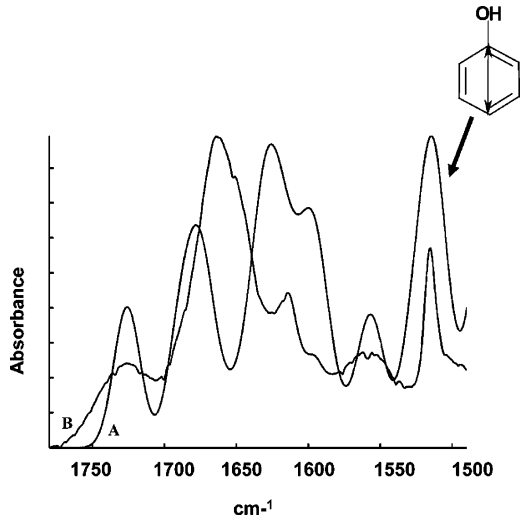

Figure 5. Infrared spectra of KTP from theoretical calculations (A) and experimental determination at [KTP] = 10 mg/mL on a germanium plate (B). The transition moment orientation of the band at 1515 cm^{-1} is depicted. The vertical arrow denotes the ^1L_a transition, and the ^1L_b transition is perpendicular to this one.

cholesterol to KTP (or KTP-K-palmitoyl) were 2.5:1 and 1.5:1:1, respectively, as in UV−vis linear dichroism studies. Aligned lipid multilayers preparation was also as in UV−vis linear dichroism studies. Measurements were carried out at room temperature. The software used for data processing was written under MatLab 6.5 (Mathworks, Inc., Natick, MA).

A more detailed description of the data analysis methodologies can be found elsewhere.[42,43] Second rank order parameters are calculated from the IR absorption of a selected band at 1515 cm^{-1} with orthogonal incident beam polarizations. The simulated kyotorphin molecular conformation and correspondent spectral assignments (see description in this section) showed that this band corresponds to C−H in-plane bending in the phenolic ring, which has an associated transition moment that is perpendicular with respect to the one that is observed in fluorescence studies (^1L_b transition). The different theoretical spectra obtained for each proposed conformation were multiplied by the percentage of its occurrence. The spectra were added, and the resulting spectrum was multiplied by a normalization factor of 0.9806.[41] This spectrum was compared with the experimental spectrum (Figure 5), and a match between theoretical and experimental bands of tyrosine (1515 cm^{-1}) and amide II (1550 cm^{-1}) was achieved. This allowed us to obtain the associated $\langle P_2 \rangle$ and obtain the overall orientation of the phenolic ring in KTP and KTP-K-palmitoyl.

3. Results and Discussion

3.1. Cluster Analysis of the Simulated Trajectories. As any small peptide, KTP displays a large number of conformations in solution, as shown by the results of the simulations. However, its conformation is not completely random, and the simulations show significant structural features. Four different conformational clusters were found in the simulation of KTP with the N-terminus neutral. These can be appreciated in Figure 4. Clearly, the most predominant conformation (approximately one-third of the time), represented in Figure 4a, is a conformation where the side chains of the tyrosine and arginine are "folded" against each other, avoiding water and creating a rather compact structure. The conformation represented in Figure 4b can be considered an extended conformation. Conformations present in Figures 4c and 4d both have a hydrogen bond between the guanidyl group of arginine and the neutral N-terminus, which can serve as a proton acceptor. These two conformations basically differ in the orientation of the side chain of tyrosine. When the N-terminus is protonated (charged), the conformational space of KTP is rather different, and extended conformations dominate (results not shown but similar to the conformation present in Figure 4b). These extended conformations keep the N- and C-terminus far apart, which seems to be, at first analysis, a contradictory result given that these opposite charges should attract each other. However, in dipeptides, charge solvation by water is usually stronger than this attraction, "pushing" the two termini into the solution (unpublished results). Whatever the effect, these conformational differences upon changes in the protonation state are very important in determining the conformation of KTP and possibly its biological function.

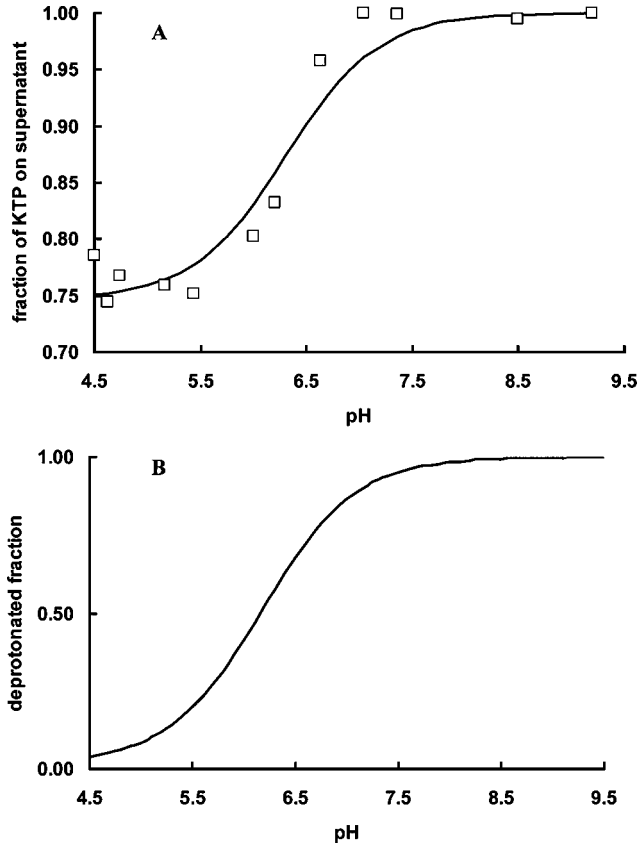

Figure 6. Experimental (A) and theoretical (B) titration curves of kyotorphin. Solid line in A represents fitting of eq 8 to the data (□).

3.2. Studies in Aqueous Solution. The "real" global charge of small peptides at a desired pH is a problem often neglected. However, formal net charges may not be realistic. At biological pH (7.4) KTP has a neutral global charge in contrast with expectation from formal charges for each amino acid individually. An experimental pK_a of 6.2 (see curve in Figure 6) was obtained for KTP. The end result of the pH titration of KTP using the LRA approach, described in the Materials and Methods section, can be seen in Figure 6b. The calculated value in molecular dynamics simulations is 6.2, which correlates very well with the experimental results, showing the validity of this approach and clearly identifying the N-terminus as the group titrating close to physiological pH. This low value for the α-amine group (in free amino acids is approximately 9 and in proteins is around 7.5) is not surprising, and it is due to interactions with other groups in the molecule. Nevertheless, the N-terminus is predominantly deprotonated at pH 7, with a small percentage in the protonated form. Therefore, KTP is

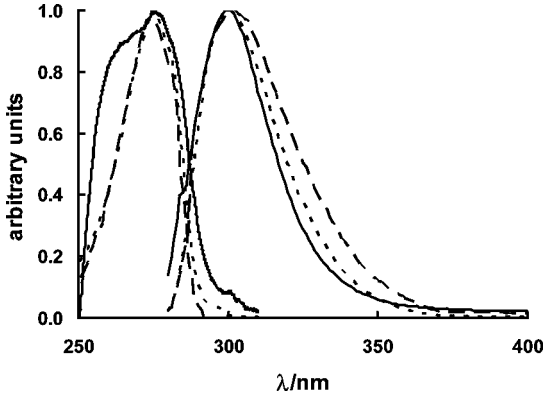

Figure 7. KTP (— — —), KTP-K-palmitoyl (—), and L-Tyr (- - - -) normalized absorption and fluorescence emission spectra ($\lambda_{exc} = 277$ nm) in the buffer Bis−Tris propane 20 mM and pH 7.4.

TABLE 1: Photophysical Parameters for L-Tyr, KTP, and KTP-K-Palmitoyl in Buffer Bis−Tris Propane 20 mM and in Large Unilamellar Vesicles (5 mM) at pH 7.4[a]

parameters	L-Tyr	KTP	KTP-K-palmitoyl
λ_{abs}/nm	275[b]	275	276
λ_{em}/nm	303[b]	303	300
$\Phi_{F,W}$	0.14[b]	0.028	
$\Phi_{F,L}$		0.036	
$\bar{\tau}_W$ (ns)	3.6[b]	1.6	0.7
$\bar{\tau}_L$ (ns)		2.7	4.6

[a] λ_{abs} and λ_{em} are the maximum absorption and emission wavelengths, respectively. Φ_F is the fluorescence quantum yield, and $\bar{\tau}$ is the mean fluorescence lifetime. [b] At 23 °C in aqueous solution and neutral pH in ref 23.

predominantly neutral at this pH, which may be a crucial factor for its mode of action (see Conclusions section).

Absorption and emission spectra of KTP and KTP-K-palmitoyl in solution are shown in Figure 7. Except for KTP-K-palmitoyl, the spectra obtained are similar to the ones obtained with free L-tyrosine in solution (Table 1). The wider absorption band observed is probably due to the hydrophobic fatty acid chain of KTP-K-palmitoyl, which may induce aggregation and exciton interaction even at such a low concentration (70 μM),[44] as observed with the phenolic-related chromophores of Triton X-100[45] due to clustering.

The photophysical parameters summarized in Table 1 show that despite the fact that the maximum absorption and emission wavelengths of the peptides are maintained relative to L-Tyr, the fluorescence quantum yield (Φ_F) and mean lifetime ($\bar{\tau}$) are smaller. Several authors[46,47] have suggested that the fluorescence of an aromatic amino acid side chain can be quenched by the peptide group as a consequence of a charge transfer between the excited chromophore (phenol ring), acting as a donor, and electrophilic units in the amino acid backbone, acting as an acceptor. Moreover, Ross et al.[48] also observed that if the phenol side chain is shielded from solvent and the local environment contains no proton acceptors, then many intra- and intermolecular interactions result in a reduction of the quantum yield.[48]

3.3. Partition Studies in LUV. The fluorescence quantum yield and mean excited-state lifetime of KTP increases in the presence of LUV relative to homogeneous aqueous solution (Figure 2). This is a clear indication that the phenolic ring is interacting with the lipidic vesicles. Three major factors seem to govern KTP partition to lipidic systems: peptide charge, lipid phase, and cholesterol presence/absence (Table 2).

To study the influence of peptide charge in partition, we have chosen to carry out experiments at pH 4.94 and pH 7.4, at which the dipeptide has a global net charge of approximately +1 and 0, respectively. At both pH 4.94 and pH 7.4, with a salt concentration of 20 mM, most 1-palmitoyl-2-oleoyl-phosphatidylglycerol (POPG) is fully deprotonated,[49,50,51] having a −1 net charge in its polar headgroup, while 1-palmitoyl-2-oleoyl-*sn*-glycero-3-phosphocholine (POPC) is a zwitterionic lipid. A global net charge of +1 (pH 4.94) favors KTP partition into lipids, in both POPC and POPG. While the effect in POPG is not surprising, due to electrostatic attraction, the result obtained in POPC makes it clear that electrostatic attraction is not the only factor governing partition, as observed before for other dipeptide drugs,[52] where conformational effects are of major importance,[52] together with structural requirements of the host matrix where dipeptides are to be inserted.[53] A detailed explanation for the lower partition coefficient, K_p, in POPG compared to POPC is thus not attainable. However a direct effect of the phenolic ring in-depth location correlated with charge effects can be speculated. At pH 4.94, KTP has, in its structure, two positive charges (one in the side chain of the arginine residue and another in the α-amino group of the tyrosine residue) and one negative charge (in the α-carboxyl terminus). Interfacial partitioning of arginine has been assumed to be relatively favorable due to the hydrophobic interaction of their methylenes with the membrane interface while the charged groups would have unfavorable contributions and interact with the aqueous phase.[54] In both cases, in negatively charged bilayers, the extra positive charge hinders a more in-depth location in the bilayer, forcing the projection of the phenol ring to the aqueous phase (and putatively a different conformation), which would be translated to a decrease in the observed K_p values.

At pH 7.4 KTP is globally neutral, possessing one positive charge in the side chain of the arginine residue and one negative charge in the α-carboxyl terminus. Consequently, an increased negative membrane surface charge has no significant extra uptake effect on the binding of the neutral KTP (Table 2). Similar K_p values for KTP in POPC and POPG membranes are observed for similar conditions at pH 7.4 (Table 2).

KTP prefers gel crystalline phase systems to liquid crystalline ones at biological pH; K_p in dipalmitoylphosphatidylcholine (DPPC) is higher than those in POPC and POPG vesicles (Table 2). Cholesterol addition to liquid crystalline phase systems increases the partition coefficient (Table 2), which is expected from its condensation effect in light of the results obtained with DPPC. Condensation is mainly achieved by an enhancement of van der Waals interactions between adjacent lipid molecules and a consequent decrease in the average molecular area of the lipid in the bilayer surface. Lipidic acyl chains become more ordered, which causes a drying effect in the lipid/water interface. Apparently increased negative surface charge has no significant effect on the binding of globally neutral KTP to cholesterol-containing systems at pH 7.4 (Table 2) since similar K_p values are obtained for POPC + cholesterol and POPG + cholesterol sytems. Thus, bilayer fluidity, but not lipid charge, seems to be the key issue in partition extension regulation at physiological pH. KTP seems to be able to discriminate between patches of membranes having different rigidities, e.g., lipidic rafts. This may be one of the key features and one of the biophysical foundations of its action, namely, in "finding the way" toward receptors, which are usually anchored to membranes by means of lipidic rafts.

KTP-K-palmitoyl behaves similarly to KTP in many aspects (Table 2) with the advantage of a greater partition extent to LUVs at both pH values due to the anchoring effect of the hydrophobic group. This is a first indication that KTP-K-

TABLE 2: Partition Coefficient Constant (K_p), Stern−Volmer Constant (K_{SV}), Fraction of Fluorescence Intensity Emitted from Peptides in the Lipidic Environment (f_L) and Fraction of Fluorescence Intensity Accessible to Each Quencher (f_B) for KTP and KTP-K-Palmitoyl in Different Lipid Systems[a]

system	cholesterol	$K_p \times 10^3$ KTP	$K_{SV} \times 10^{-3}/M^{-1}$ KTP	f_L KTP	f_B KTP	$K_p \times 10^3$ KTP-K-palmitoyl
POPC pH 4.94	−	10.3 ± 3		0.83		13.0 ± 2
	+	15.0 ± 4	7.02 ± 0.77	0.89	0.23 ± 0.01	
POPG pH 4.94	−	2.5 ± 0.5		0.97		11.0 ± 5
	+	5.9 ± 2.3	6.23 ± 0.88	0.98	0.63 ± 0.02	
POPC pH 7.4	−	0.66 ± 0.23	0.11 ± 0.02	0.75	0.99 ± 0.02	8.4 ± 1.0
	+	1.2 ± 0.4	8.06 ± 1.8	0.90	0.27 ± 0.01	
DPPC pH 7.4	−	1.1 ± 0.5				
POPG pH 7.4	−	0.61 ± 0.25	0.12 ± 0.03	0.77	0.99 ± 0.01	6.7 ± 2.2
	+	1.7 ± 2.3	15.4 ± 0.32	0.9(9)	0.31 ± 0.01	

[a] Minus and plus, in the cholesterol column, denote the absence or presence of cholesterol (33 mol %), respectively. Iodide and cholesteryl bromide were used as quenchers in the systems with and without cholesterol, respectively.

palmitoyl might mimic KTP properties and potentiate its use, since it is easier to entrap in drug carriers, such as liposomes.

3.4. KTP Location in LUVs. Fluorescence quenching studies were performed to further confirm KTP's phenolic ring location in the different systems. Cholesteryl bromide and iodide anions were used as quenchers of KTP fluorescence in the presence of bilayers with or without cholesterol, respectively. The ability of the quenchers to decrease tyrosine fluorescence can be used to conclude on the degree of exposure of this amino acid residue to the aqueous phase or lipidic interface. I^- is able to quench tyrosine residues that are exposed to the aqueous phase. The bromide (quencher) in cholesteryl bromide is replacing the −OH group in cholesterol and is putatively at the same depth in the lipidic bilayer interface, being thus able to quench phenolic rings at this depth. If the fluorophore is exposed to the aqueous medium, then a considerable fraction of the emitted fluorescence will be quenched by I^-; however, if it is buried in the lipidic headgroup interface (i.e., in the quencher vicinity), then quenching by cholesteryl bromide will be effective. Insertion deep in the core of the membrane would lead to no quenching by either. The fraction of fluorescence intensity accessible to each quencher (f_B) was determined from application of the Lerher equation (eq 14), while the fraction of fluorescence intensity emitted from the lipidic environment (f_L) was determined from K_p (eq 11). From Table 2 it is clear that almost all fluorescence signals are from peptides that are interacting with the lipidic bilayer, since f_L is always ≥ 0.75. Moreover, in systems without cholesterol, the tyrosine ring in KTP is fully exposed to the aqueous phase, $f_B \cong 1$. When cholesterol is added to the different systems and despite the fact that its condensation effect promotes peptide interaction with lipids (K_p and f_L increase), only a small part of the tyrosine residues are quenched by cholesteryl bromide. This means that only a small part of the dipeptide population is buried deeper in the lipidic headgroup interface while the remaining in a superficial location in the membrane. Therefore, a high degree of exposure of the tyrosine ring in KTP to the aqueous phase bulk environment is concluded, in both cholesterol-free and cholesterol-rich lipidic membranes. The shallow location makes the phenolic ring of tyrosine exposed and accessible for molecular recognition through cellular receptor-mediated processes.

3.5. KTP and KTP-K-Palmitoyl Orientation in Multibilayers. The lowest energy singlet transition of tyrosine is due to the ^1L_b transition, oriented across the phenyl ring (Figure 5), with an absorption maximum of approximately 277 nm.[23] If the excitation radiation wavelength is >260 nm, then absorption and emission occur from the same ^1L_b state, and orientation of the peptide phenolic ring can be obtained from UV−vis linear dichroism methodologies. We used UV−vis linear dichroism and ATR-FTIR studies to obtain the orientation of the tyrosine ring in membrane-inserted KTP and KTP-K-palmitoyl. The $\langle P_2 \rangle$ values obtained from UV−vis linear dichroism (Table 3) report the orientation of the ^1L_b moment, and the $\langle P_2 \rangle$ values calculated from ATR-FTIR measurements (Table 4) report the orientation of a transition moment that is perpendicular to ^1L_b (Figure 5), both relative to the bilayer normal. Both sets of $\langle P_2 \rangle$ values are in agreement, taking into account that both transition moments are displaced by 90°.[28] The second rank order parameters suggest that phenolic rings are at an intermediate position between perpendicular and parallel to the lipidic membrane surface. Peptide charge seems to have apparently the effect of decreasing, on average, the angle between the bilayer normal (system director axis) and both phenolic transition moments when we look to the $\langle P_2 \rangle$, suggesting that the whole phenolic ring plan comes closer to the membrane surface rather than performing a in-plane rotation toward the membrane surface (which would decrease one of the $\langle P_2 \rangle$ values while increasing the other); see Figure S1 in the Supporting Information. In the cases where a $\langle P_4 \rangle$ can be calculated and thus probability density functions are determined (Figure 8), an average angle of 13−27° relative to the membrane normal is obtained. Except when membranes of POPG are used, orientational probability distribution functions are fairly narrow. One can conclude that not only

TABLE 3: Second ($\langle P_2 \rangle$) and Fourth ($\langle P_4 \rangle$) Rank Order Parameters Obtained by UV−Vis Linear Dichroism for KTP and KTP-K-Palmitoyl in Different Lipid Systems[a]

system	cholesterol	$\langle P_2 \rangle$ KTP	$\langle P_4 \rangle$ KTP	$\langle P_2 \rangle$ KTP-K-palmitoyl
POPC pH 4.94	−	0.600		0.684
	+	0.600	0.557	
POPG pH 4.94	−	0.769	0.334	0.647
	+	0.704	0.334	
DPPC pH 7.4	−	0.632		
POPC pH 7.4	−	0.692	0.721	0.666
	+	0.488		
POPG pH 7.4	−	0.327		0.640
	+	0.530		

[a] Minus and plus, in the cholesterol column, denote the absence or presence of cholesterol (33 mol %), respectively.

TABLE 4: Second Rank Order Parameter ($\langle P_2 \rangle$) Obtained, from ATR-FTIR Studies, for KTP and KTP-K-Palmitoyl in Different Lipid Systems at pH 4.94 and pH 7.4

system	KTP	KTP-K-palmitoyl
DPPC pH 4.94	0.464	0.561
DLPC[a] pH 4.94	0.464	0.561
DPPG[b] pH 4.94	0.464	0.464
DPPC pH 7.4	0.380	0.250
DLPC[a] pH 7.4	0.380	0.250
DPPG[b] pH 7.4	0.250	0.120

[a] Dilauroylphosphocholine. [b] Dipalmitoylphosphatidylglycerol.

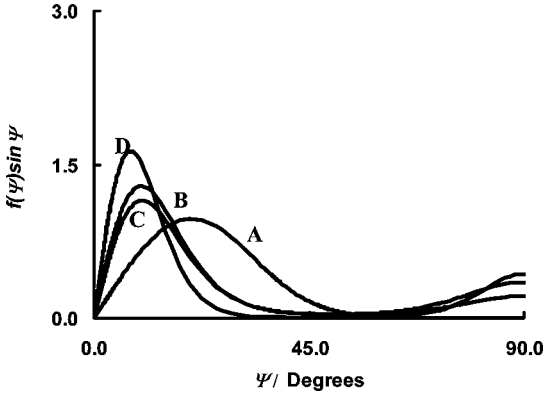

Figure 8. Orientational probability density functions of KTP at room temperature, pH 4.94, in multibilayers of POPG (A), POPG + cholesterol (B), POPC + cholesterol (C), and at pH 7.4 in POPC multilayers (D).

the tyrosine ring has a defined orientation but also that the orientation is rather insensitive to membrane properties. The hydrophobic analogue, KTP-K-palmitoyl, has showed similar behavior in similar conditions to those used for KTP. So, it not only partitioned in greater extent to model membranes but also has the same orientation of KTP in membranes.

4. Conclusions

KTP interacts with the model systems of biological membranes, despite its strong hydrophilic character. Experimental and simulation data show that the pK_a of KTP is ~6.2. Although the interaction is more effective when the peptides have a +1 global charge (pH 4.94), at biological pH (7.4) at least 70% of the peptide population is in contact with the lipid, in all of the studied systems. At biological pH KTP prefers gel crystalline phase systems. A superficial location of the phenolic ring of tyrosine was concluded, mainly in cholesterol-free membranes. Phenolic groups are common and essential in many biological active peptides and are involved in the interaction with cell receptors (e.g., enkephalins, endorphins, and related molecules).[19] Exposure and orientation are therefore crucial for molecular recognition trough cellular receptor-mediated processes. The present study demonstrates that the phenolic ring of KTP is exposed for receptor interaction with a well-defined orientation relative to the bilayer plane. Although KTP locates preferably in raftlike domains in membranes, orientation is rather insensitive to the membrane phase. None of the most frequent conformations in bulk aqueous medium meet the spatial structure requirements needed for active interaction with receptors. However, it can be speculated that membranes may induce a favorable conformation for receptor docking. This hypothesis is further developed in the Supporting Information.

Acknowledgment. The authors acknowledge the Fundação para a Ciência e Tecnologia (Portugal) for funding and Grant No. SFRH/BD/6497/2001 to S. Lopes. Dr. Goormaghtigh is Research Director of the Belgian National Fund for Scientific Research.

Supporting Information Available: UV−vis linear dichroism studies, molecular dynamics simulations of conformers and ionization states, and membrane−receptor docking of KTP. This material is available free of charge via the Internet at http://pubs.acs.org.

References and Notes

(1) Takagi, H.; Shiomi, H.; Ueda, H.; Amano, H. *Nature* **1979**, *282*, 410−412.
(2) Ueda, H.; Shiomi, H.; Takagi, H. *Brain Res.* **1980**, *198*, 460−464.
(3) Shiomi, H.; Ueda, H.; Takagi, H. *Neuropharmacology* **1981**, *20* (7), 633−638.
(4) Inoue, M.; Yamada, T.; Ueda, H. *Mol. Brain Res.* **1999**, *69* (2), 302−305.
(5) Takagi, H.; Shiomi, H.; Ueda, H.; Amano, H. *Eur. J. Pharmacol.* **1979**, *55* (1), 109−111.
(6) Stone, T. W. *Br. J. Pharmacol.* **1983**, *79*, 305−312.
(7) Rackham, A.; Wood, P. L.; Hudgin, R. L. *Life Sci.* **1982**, *30*, 1337−1342.
(8) Ueda, H.; Yoshihara, Y.; Misawa, H.; Fukushima, N.; Katada, T.; Ui, M.; Takagi, H.; Satoh, M. *J. Biol. Chem.* **1989**, *264* (7), 3732−3741.
(9) Ochi, T.; Motoyama, Y.; Goto, T. *Life Sci.* **2000**, *23*, 2239−2245.
(10) Shiomi, H., Kuraishi, Y.; Ueda, H.; Harada, Y.; Amano, H.; Takagi, H *Brain Res.* **1981**, *221* (1), 161−169.
(11) Arima, T.; Kitamura, Y.; Nishiya, T.; Taniguchi, T.; Takagi, H.; Nomura, Y. *Neurochem. Int.* **1997**, *30* (6), 605−611.
(12) Inoue, M.; Nakayamada, H.; Tokuyama, S.; Ueda, H. *Neurosci Lett.* **1997**, *236* (1), 60−62.
(13) Bronnikov, G.; Dolgacheva, L.; Zhang, S. J.; Galitovskaya, E.; Kramarova, L.; Zinchenko, V. *FEBS Lett.* **1997**, *407*, 73−77.
(14) Chen, P.; Bodor, N.; Wu, W.-M.; Prokai, L. *J. Med. Chem.* **1998**, *41*, 3773−3781.
(15) *Bioavailability of Drugs to the Brain and the Blood−Brain Barrier*; Frankenheim, J., Brown, R. M., Eds.; Research Monograph 120; Natural Institute on Drug Abuse: Rockville, MD, 1992; pp 121−137.
(16) Sargent, D. F.; Schwyzer, R. *Proc. Natl. Acad. Sci. U.S.A.* **1986**, *83*, 5774−5778.
(17) Abdiche, Y. N.; Myszka, D. G. *Anal. Biochem.* **2004**, *328*, 233−243.
(18) Kabanov, A. V.; Batrakova, E. V. *Curr. Pharm. Design* **2004**, *10*, 1−9.
(19) Patrick, G. L. *An Introduction to Medicinal Chemistry*, 2nd ed.; Oxford University Press: New York, 2001; pp 511−550.
(20) Fery-Forgues, S.; Lavabre, D. *J. Chem. Educ.* **1999**, *76*, 1260−1264.
(21) Gjerde, D. T.; Fritz, J. S. Ion-exchange selectivity and distribution coefficients. In *Ion Chromatography*, 2nd ed.; Hüthig: Berlin, 1987; pp 63−76.
(22) Hope, M. J.; Bally, M. B.; Webb, G.; Cullis, P. R. *Biochim. Biophys. Acta* **1985**, *812*, 55−65.
(23) Lakowicz J. R. Proteins fluorescence. In *Principles of Fluorescence Spectroscopy*, 2nd ed.; Kluwer Academic, Plenum Publishers: New York, 1999; pp 445−486.
(24) Santos, N. C.; Prieto, M.; Castanho, M. A. R. B. *Biochim. Biophys. Acta* **2003**, *1612*, 123−135.
(25) Castanho, M. A. R. B.; Prieto, M. J. E. *Biochim. Biophys. Acta* **1998**, *1373*, 1−16.
(26) Castanho, M. A. R. B., Prieto, M. J. E. *Biophys. J.* **1995**, *69*, 155−168.
(27) Leher, S. S. *Biochemistry* **1971**, *10*, 3254−3263.
(28) Castanho, M. A. R. B.; Lopes, S.; Fernandes, M. *Spectrosc. Int. J.* **2003**, *17*, 377−398.
(29) Dyson, H. J.; Wright, P. E. *Annu. Rev. Biophys. Biophys. Chem.* **1991**, *20*, 519−538.
(30) Aburi, M.; Smith, P. E. *Biopolymers* **2002**, *64*, 177−188.
(31) Bashford, D. *Front. Biosci.* **2004**, *9*, 1082−1099
(32) Warshel, A.; Russell, S. T.; Churg, A. K. *Proc. Natl. Acad. Sci. U.S.A.* **1984**, *81*, 4785−4789.
(33) Schutz, C. N.; Warshel, A. *Proteins* **2001**, *44*, 400−417.
(34) Sham, Y. Y.; Muegge, I.; Warshel, A. *Biophys. J.* **1998**, *74*, 1744−1753.
(35) Sham, Y. Y.; Chu, Z. T.; Warshel, A. *J. Phys. Chem.* **1997**, *101*, 4458−4472.
(36) Eberini, I.; Baptista, A. M.; Gianazza, E.; Fraternali, F.; Beringhelli, T. *Proteins* **2004**, *54* (4), 744−58.
(37) Parr, R. G.; Yang, W. *Density Functional Theory of Atoms and Molecules*; Oxford University Press: Oxford, U. K., 1989.
(38) Becke, A. D. *J. Chem. Phys.* **1993**, *98*, 5648−5652.
(39) Lee, C. T.; Yang, W. T.; Parr, R. G. *Phys. Rev. B* **1988**, *37*, 785−789.
(40) Binning, R. C.; Curtiss, L. A., Jr. *J. Comput. Chem.* **1990**, *11*, 1206−1216.
(41) Montgomery, J. A., Jr.; Frisch, M. J.; Ochterski, J. W.; Petersson, G. A. *J. Chem. Phys.* **1999**, *110*, 2822−2827.
(42) Bechinger, B.; Ruysschaert, J. M.; Goormaghtigh, E. *Biophys. J.* **1999**, *76*, 552−563.
(43) Goormaghtigh, E.; Raussens, V.; Ruysschaert, J. M. *Biochim. Biophys. Acta* **1999**, *1422*, 105−185.
(44) Cantor, C. R.; Schimmel, P. R. *Biophysical Chemistry: Techniques for the Study of Biological Structure and Function*; W. H. Freeman & Company: New York, 1980; Part II, pp 390−398.

(45) Kalyanasundaram, K.; Thomas, J. K. In *Symposium on Micellization, Solubilization, and Microemulsions*; Miltal, K. L., Ed.; New York: Plenum Press, 1977; Vol. 2, pp 559−589.
(46) Tournon, J. E.; Kuntz, E.; El Bayoumi, M. A *Photochem. Photobiol.* **1972**, *16*, 425−433.
(47) Guzow, K.; Ganzynkowicz, R.; Rzeska, A.; Mrozek, J.; Szabrlski, M.; Karolczak, J.; Liwo, A.; Wiczk, W. *J. Phys. Chem. B* **2004**, *180*, 3879−3889.
(48) Ross, J. B. A.; Laws, W. R.; Rousslang, K. W.; Wyssbrod, H. R. Tyrosine fluorescence and phosphorescence from proteins and polypeptides. In *Topics in Fluorescence Spectroscopy*; Lakowicz, J. R., Ed.; Plenum Press: New York, 1992; Vol. 3, pp 1−63.
(49) Träuble, H.; Teubner, M.; Woolley, P.; Eibl, H. *Biophys. Chem.* **1976**, *4*, 319−342.
(50) Van Dijck, P. W. M.; De Kruihff, B.; Verkleij, A. J.; Van Deenen, L. L. M.; De Gier, J. *Biochim. Biophys. Acta* **1978**, *512*, 84−96.
(51) Watts, A.; Harlos, K.; Maschke, W.; Marsh, D. *Biochim. Biophys. Acta* **1978**, *510*, 63−74.
(52) Kloosterman, D. A.; Goodwin, J. T.; Burton, P. S.; Conradi, R. A.; Stockman, B. J.; Scahill, T. A.; Blinn, J. R. *Biopolymers* **2000**, *53* (5), 396−410.
(53) Bombelli, C.; Borocci, S.; Lupi, F.; Mancini, G.; Mannina, L.; Segre, A. L.; Viel, S. *J. Am. Chem. Soc.* **2004**, *126* (41), 13354−13362.
(54) Wimley, W. C.; White, S. H. *Nat. Struct. Biol.* **1996**, *3*, 842−848.